Synthesis, Phase Stability, and Electrochemically Driven Transformations in the LiCuO$_2$−Li$_2$CuO$_2$ System

A. S. Prakash,[†] D. Larcher,*,[†] M. Morcrette,[†] M. S. Hegde,[‡] J-B. Leriche,[†] and
C. Masquelier[†]

*Laboratoire de Réactivité et Chimie des Solides, CNRS UMR 6007, 33, rue Saint Leu, Université de
Picardie Jules Verne, 80039 Amiens, France, and Solid State and Structural Chemistry Unit,
Indian Institute of Science, Bangalore, India, 560 012*

Trivalent LiCuO$_2$ was prepared by oxidative leaching of divalent Li$_2$CuO$_2$ in Br$_2$-acetonitrile solutions at ambient temperature. Both phases were found to be thermally air unstable and the onset temperatures (100−150 °C) relatively low for their transformation into CuO and lithium salts. Electrochemically driven lithium insertion/ extraction into/from both Li$_2$CuO$_2$ and LiCuO$_2$ were followed by in situ X-ray diffraction that revealed, for both starting materials, that the Li$_2$CuO$_2$ ⇆ LiCuO$_2$ transitions always proceed through a succession of biphasic and monophasic processes involving three type phases: Li$_{1+y}$CuO$_2$, "Li$_{1.5}$CuO$_2$", and Li$_{2−z}$CuO$_2$. Such a strategy can therefore be used for the preparation of stable copper mixed valence oxides. This study also revealed a very large polarization linked to the Li$_{1.5}$CuO$_2$ → Li$_2$CuO$_2$ transition. Although so far not explained, this fact enabled us to test the respective reversibility of the LiCuO$_2$ ⇆ Li$_{1.5}$CuO$_2$ and Li$_{1.5}$CuO$_2$ ⇆ Li$_2$CuO$_2$ transitions. It was found that performing cycling on both transitions comes with a continuous decrease in the cell capacity while good capacity retention can be obtained when one limits the electrochemical work to the LiCuO$_2$ ⇆ Li$_{1.5}$CuO$_2$ process.

Introduction

Since the late 1970s, lithiated 3d metal oxides have attracted a sustained interest among electrochemists as positive electrode materials for Li ion battery.[1−4] Besides 3D Li$_{1+x}$Mn$_{2−x}$O$_4$ spinel materials, 2-D layered compounds such as LiNiO$_2$ and LiCoO$_2$ were extensively studied and optimized, the latter being now universally implemented in commercialized secondary cells.

Superconductivity, magnetic, and electrical properties of Cu-based compounds with mixed valence have aroused much interest, unlike layered copper oxides whose electrochemical activity has rarely been investigated.[5−7] However, the Li−Cu−O system is known to contain numerous defined phases including Li$_2$CuO$_2$, Li$_3$Cu$_2$O$_4$ (Li$_{1.5}$CuO$_2$), LiCu$_2$O$_2$, and LiCuO$_2$, showing various Li/Cu ratios and Cu oxidation states.[8−12]

X-ray and neutron diffraction showed that LiCuO$_2$ (C2/m, a = 5.733 Å, b = 2.7176 Å, c = 5.622 Å, β = 120.68°) is isostructural with layered NaCuO$_2$[13] whereas Li$_2$CuO$_2$ crystallizes in the *Immm* orthorhombic space group with a = 3.654 Å, b = 2.859 Å, and c = 9.374 Å.[14] Both LiCuO$_2$ and Li$_2$CuO$_2$ structures contain infinite chains of edge-sharing planar and square CuO$_4$ units, these chains being separated/linked by LiO$_6$ octahedra (LiCuO$_2$) or LiO$_4$ tetrahedra (Li$_2$CuO$_2$) layers (Figure 1). They run parallel along the [010]$_{mono}$ axis for LiCuO$_2$, and along the [010]$_{ortho}$ direction for Li$_2$CuO$_2$. Based on the crucial impact of the mean Cu oxidation state on the possible superconducting and magnetic behavior of its oxides, the preparation of such a single phase with mixed valence is a key point. This was first achieved by Klemm et al.[9] while the structure of this Li$_{1.5}$CuO$_2$ compound was more recently solved by both X-ray[15] and neutron diffraction.[16] This phase crystallizes in the C2/m space group (a = 9.954 Å, b = 2.7772 Å, c = 7.274 Å, β = 118.697°) with similar and parallel [CuO$_2$]$_\infty$ chains running along [010] and separated by Li−O layers. The latter consist of alternate double chains of LiO$_4$ tetrahedra and single chains of LiO$_6$ octahedra, each CuO$_4$ square unit sharing one edge with one tetrahedron and one octahedron. Figure 1 shows a comparison of these three structures.

The preparation of LiCuO$_2$ from Li$_2$CuO$_2$ can be achieved through chemical oxidation of the divalent material in either

* To whom correspondence should be addressed.
† Université de Picardie Jules Verne.
‡ Indian Institute of Science.
(1) Mizushima, K.; Jones, P. C.; Wiseman, P. J.; Goodenough, J. B. *Mater. Res. Bull.* **1980,** *15,* 783−789.
(2) Thackeray, M. M.; David, W. I. F.; Bruce, P. G.; Goodenough, J. B. *Mater. Res. Bull.* **1983,** *18,* 461−472.
(3) Dahn, J. R.; Von Sacken, U.; Juzkow, M. W.; Al-Janaby, H. *J. Electrochem. Soc.* **1991,** *138,* 2207−2211.
(4) Tarascon, J-M.; Armand, M. *Nature* **2001,** *414,* 359−367.
(5) Arai, H.; Okada, S.; Sakurai, Y.; Yamaki, J.-i. *Solid State Ionics* **1998,** *106* (1−2), 45−53.
(6) Vitins, G.; Raekelboom, E. A.; Weller, M. T.; Owen, J. R. *J. Power Sources* **2003,** *119−121,* 938−942.
(7) Wizansky, A. R.; Rauch, P. E.; Disalvo, F. J. *J. Solid State Chem.* **1989,** *81,* 203−207.
(8) Imai, K.; Koike, M.; Takei, H.; Sawa, H.; Shiomi, D.; Nozawa, K.; Kinoshita, M. *J. Phys. Soc. Jpn.* **1992,** *61,* 1819.
(9) Klemm, W.; Wehrmeyer, G.; Bade, H. Z. *Elektrochem. Angew. Phys. Chem.* **1959,** *63,* 56−59.

(10) Berger, R. *J. Less-Common Met.* **1991,** *169* (1), 33−43.
(11) Hoppe, R.; Rieck, H. *Z. Anorg. Allg. Chem.* **1970,** *379* (2), 157.
(12) Hibble, S. J.; Koehler, J.; Simon, A.; Paider, S. *J. Solid State Chem.* **1990,** *88* (2), 534−542.
(13) Berger, R.; Tergenius, L.-E. *J. Alloys Compd.* **1994,** *203,* 203−207.
(14) Sapina, F.; Rodriguez-Carvajal, J.; Sanchis, M. J.; Ibanez, R.; Beltran, A.; Beltran, D. *Solid State Commun.* **1990,** *74* (8), 779−784.
(15) Berger, R.; Onnerud, P.; Laligant, Y.; Le Bail, A. *J. Alloys Comp.s* **1993,** *190* (2), 295−299.
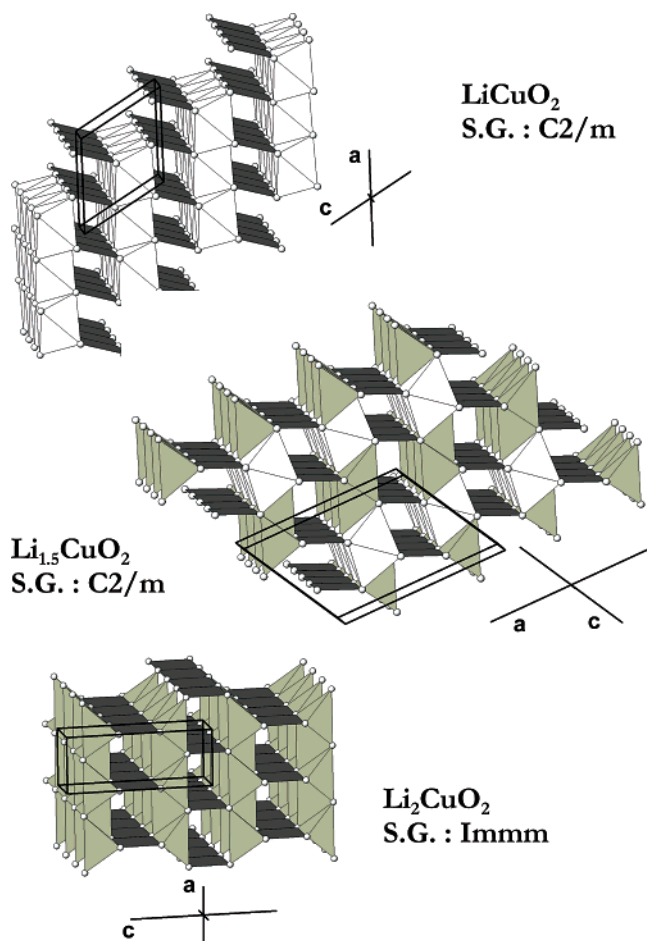(16) Currie, D. B.; Weller, M. T. *J. Mater. Chem.* **1993,** *3* (3), 229−232.

Figure 1. Schematic representations of the structures of $LiCuO_2$, $Li_{1.5}CuO_2$, and Li_2CuO_2 phases. $[CuO_4]$, $[LiO_4]$, and $[LiO_6]$ units are symbolized by black squares, gray tetrahedral, and white octahedra, respectively. White dashed spheres indicate oxygen atoms.

hot acetonitrile−I_2 solution[8] or ambient temperature acetonitrile−Br_2 solution.[13] The so-obtained products often contain small amounts of either Li_2CuO_2 due to incomplete reaction or CuO due to excess leaching. In an earlier report, oxidation of Li_2CuO_2 by a stronger oxidative agent (NO_2PF_6 solution in acetonitrile) surprisingly resulted in the formation of a mixture of Li_2CuO_2 and a phase related to $Li_{1.5}CuO_2$.[7] To our knowledge, no reliable procedure for the chemical synthesis of single-phase $LiCuO_2$ has been reported yet. Arai et al.[5] have shown the possible electrochemical formation of $LiCuO_2$ and $Li_{1.5}CuO_2$ ($Li_3Cu_2O_4$) by oxidation of Li_2-CuO_2 vs metallic lithium. Unfortunately, no accurate examination of the reaction path/mechanism was given; therefore, the intimate process and possible existence of solid solution domains still remain unknown. In addition, only partial data about the electrochemical reduction of Li_1CuO_2 are available.

To throw some light on these points, we focused our investigation on the study of these electrochemical reactions by means of in situ X-ray diffraction, galvanostatic, and potentiostatic intermittent titration techniques (GITT, PITT), together with some insights in the synthesis, thermal, and long-term stability of the Li_1CuO_2 and Li_2CuO_2 phases.

Experimental Section

Powder Synthesis. Li_2CuO_2 was prepared through a solid-state reaction between Li_2CO_3 (Aldrich, 99%) and CuO (Merck, 99%)
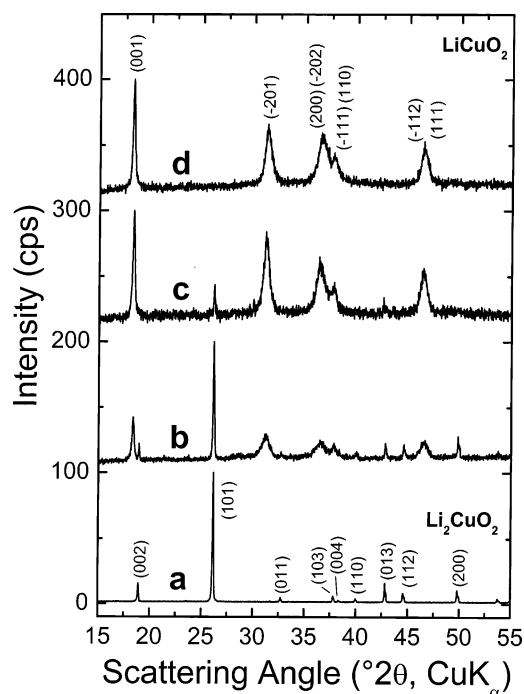

Figure 2. X-ray diffraction patterns collected for the initial Li_2CuO_2 (a) and during the three successive oxidation/leaching ambient-temperature treatments in actonitrile−Br_2 solutions (b,c,d). After the third treatment, $LiCuO_2$ is obtained. See Experimental Section for detailed conditions.
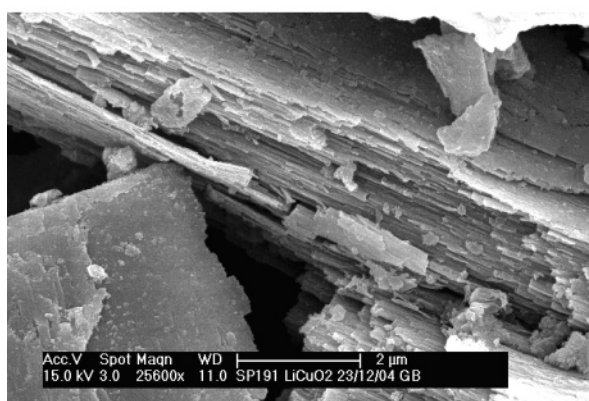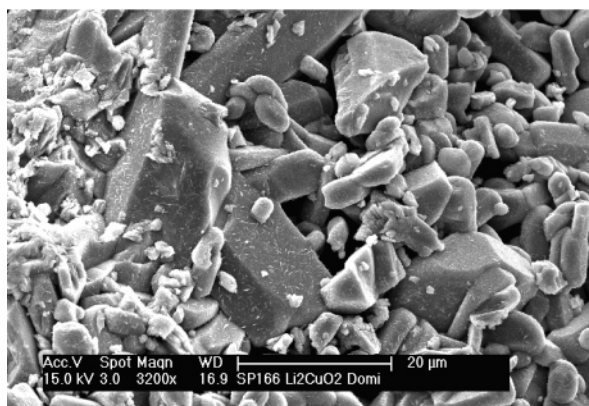

Figure 3. Scanning electron microscope (SEM) pictures of (a) powdered Li_2CuO_2 precursor and (b) resulting $LiCuO_2$ obtained by leaching/oxidation of the precursor.

using a 5% weight excess of lithium carbonate in order to avoid the formation of CuO impurity resulting from the lithium loss generally observed at high temperatures. This mixture was heated to 750 °C in static air, at a rate of 5 °C/min, maintained at this temperature for 24 h, cooled to room temperature, ground with
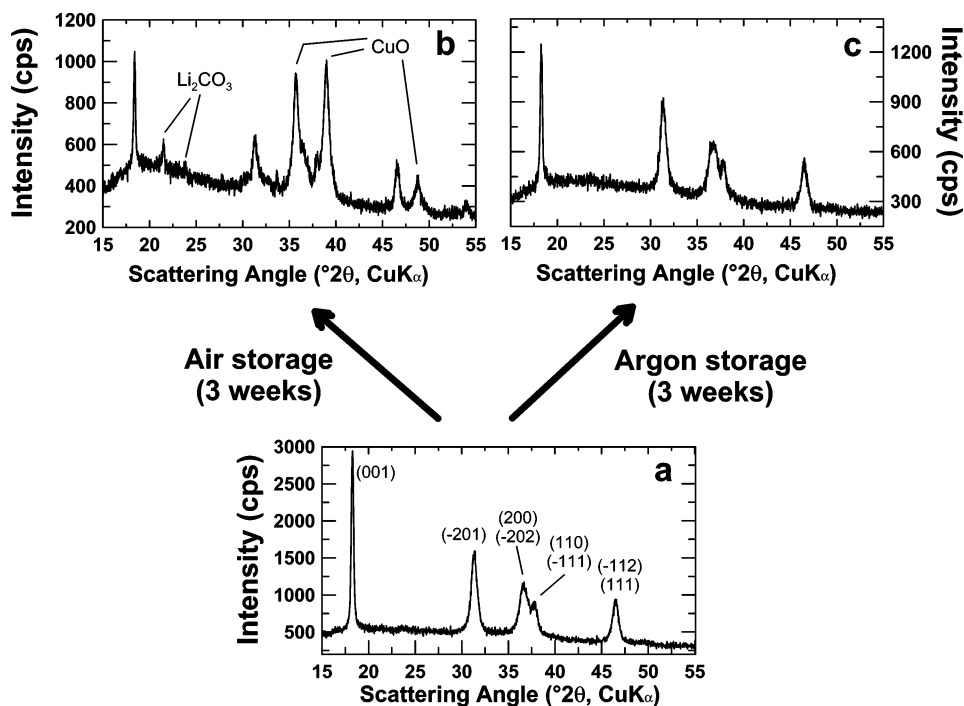
Figure 4. X-ray diffraction patterns of freshly prepared LiCuO$_2$ (a) and after 3 weeks of exposure to air (b) and argon (c) at ambient temperature.
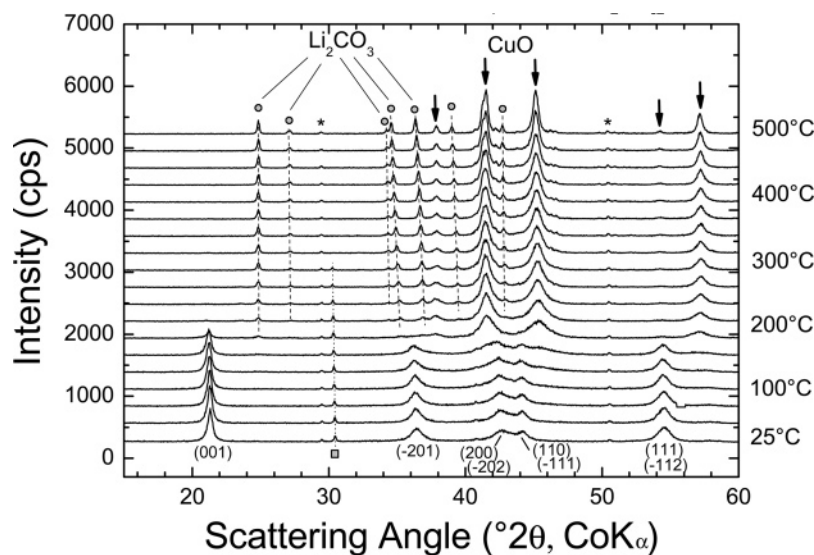

Figure 5. XRD patterns evolution during heating of LiCuO$_2$, under air at a heating rate of 6 °C/min. Reflections from sample holder (asterisk), CuO (arrow), Li$_2$CO$_3$ (circle), and Li$_2$CuO$_2$ impurity (square) are indicated.

additional 3% weight excess of Li$_2$CO$_3$, and finally annealed at 800 °C for 24 h in static air. The preparation was cooled to 500 °C and then quenched from 500 °C to room temperature to avoid the decomposition of Li$_2$CuO$_2$ (see detailed discussion later) and is now referred to as HT-Li$_2$CuO$_2$.

LiCuO$_2$ was prepared by repeated chemical lithium extraction from HT-Li$_2$CuO$_2$ using bromine solution (Aldrich, 99%) at ambient temperature. A highly reactive powder with small grain size was obtained by ball-milling 0.5 g of HT-Li$_2$CuO$_2$ for 15 min in a SPEX 8000 shock-miller using a stainless steel vial and a single stainless steel ball (7 g). The so-obtained finely divided powder was suspended and agitated in 50 mL of a 0.5 vol % (0.1 mol/L) Br$_2$ solution in dry acetonitrile (Across, 99.5%) for 30 min and then left to separate from the liquid supernatant. This process was repeated with another fresh 50 mL of Br$_2$ solution, and a third half-hour leaching was performed with 20 mL of the Br$_2$ solution diluted with 15 mL of pure and anhydrous acetonitrile, leading to a LiCuO$_2$

single-phase powder. The product was washed several times with dry acetonitrile, dried at 50 °C, and stored in an argon atmosphere.

Characterization. Routine X-ray diffraction (XRD) analyses of the powders were performed with a Philips diffractometer (PW 1710, Cu Kα, $\lambda = 1.5418$ Å) equipped with a back monochromator. Lattice parameters were refined using the Fullprof refinement software.[17] The Li/Cu atomic ratios in the various samples prepared along this study were determined by atomic absorption spectroscopy (AAS, Perkin-Elmer AAnalyst 300) after dissolution of a known amount of powder in a H$_2$O/H$_2$O$_2$/HNO$_3$ (90/5/5 v/v/v) solution. The oxidation state of copper was determined by iodometric titration.[18]

Positive electrodes were prepared by mixing 85 wt % of active material with 15 wt % SP carbon, as electronic conductor and

(17) Rodriguez-Carvajal, J. *Phys. B: Condens. Matter* **1993**, *192*, 55–69.
(18) Nazza, A. I.; Lee, V. Y.; Engler, E. M.; Jacowitz, R. D.; Tokura, Y.; Torrance, J. B. *Physica C* **1988**, *1367*, 153–155.
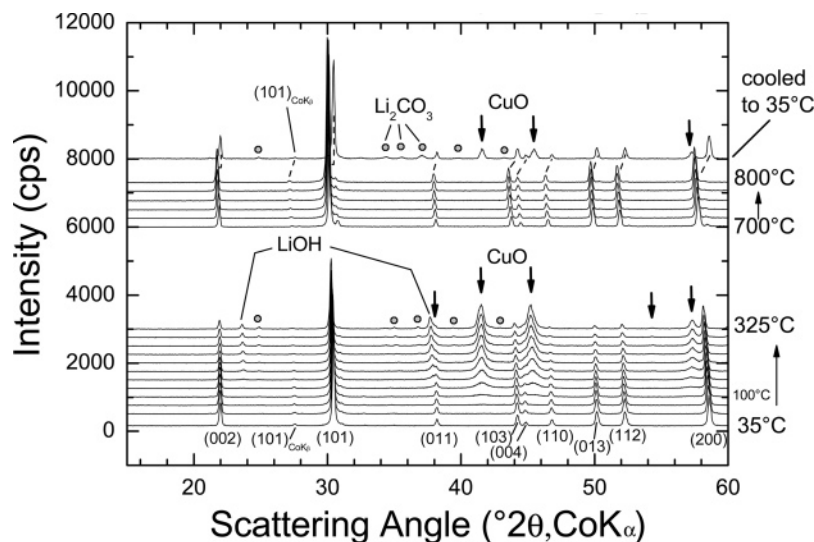
Figure 6. Evolution in XRD patterns during heating of Li_2CuO_2 under air at a heating rate of 6 °C/min. CuO (arrow), Li_2CO_3 (circle), and LiOH reflections are indicated.

Swagelok-type cells were assembled in an argon-filled glovebox. About 7 mg of the carbon/material mix was separated from the negative electrode (lithium foil) by 2 sheets of fiber glass disks, the assembly being soaked with a $LiPF_6$ (1 M) solution in an ethylene carbonate (EC)/ dimethyl carbonate (DMC) mixture (1/1 v/v). Galvanostatic tests were conducted at constant temperature (25 °C) with a Mac Pile controller at a discharge rate of 1 Li per formula unit every 5 h (noted C/5). GITT (galvanostatic intermittent titration technique) experiments were also performed to determine the quasi-equilibrium open circuit potential at various reaction levels in both Li_1CuO_2 and Li_2CuO_2 materials. The OCV (open circuit voltage) was determined once the time evolution of the voltage was lower than 3 mV/h, after reduction/oxidation steps of 0.25 h at a C/10 rate. PITT (potentiostatic intermittent titration technique) data and accurate dx/dV incremental capacities were determined by integrating the chronoamperometric curves recorded for each sample with 10 mV voltage steps and a C/20 cutoff limit current. Within the potential windows presently studied, we checked that the conductive SP carbon additive did not show any electrochemical reactivity with lithium.

The structural evolution of the electrode materials in the course of the reaction with lithium was followed by in situ XRD using a D-8 Bruker diffractometer (Co Kα, λ = 1.78897 Å, position sensitive detector) and a specially designed Swagelok cell equipped with an X-ray-transparent beryllium window also acting as a current collector. To bypass the oxidation of beryllium during high-voltage analysis, a thin layer of aluminum was deposited by evaporation onto the inner side of the window.[19] The in situ XRD patterns were collected during the charge or discharge recorded at a C/20 rate (1 Li in 20 h). High-temperature XRD experiments were carried out on the D8 diffractometer using an alumina sample holder, under open air, and with a heating rate of 6 °C/min. Because of an incomplete slit wavelength selection, small satellite reflections due to Co Kβ radiation can occasionally superimpose onto the main Co Kα pattern.

The specific surface area of our powders was calculated using the Brunauer− Emmett−Teller multipoints formalism[20] and computation of results from isothermal (77 K) nitrogen adsorption recorded with a 2375 Gemini analyzer. Prior to BET measurements,

and for the sake of intrinsic thermal instability of our materials, removal of adsorbed water/species was preferentially performed by a long treatment (several hours) at relatively low temperature (75 °C) under argon flow. We checked by XRD that no decomposition occurred during these degassing treatments.

Powder morphology/size was determined by scanning electron microscopy (SEM) observations performed with a Philips FEG XL-30 device equipped with energy dispersive spectroscopy (EDS) analysis probe (Link Isis Oxford).

Results and Discussions

Powder Synthesis and Stability. The X-ray diffraction pattern of $HT-Li_2CuO_2$ (Figure 2a) evidences no impurity (e.g., CuO) and the refined cell parameters (a = 3.660(1) Å, b = 2.861(1) Å, and c = 9.392(3) Å) are in agreement with the values reported in the literature.[14] The Li/Cu elemental analysis and the Cu oxidation state determination in $HT-Li_2CuO_2$ lead to the general formula $Li_{1.92}CuO_{1.97}$. Worth noting is that this material was found to be air-stable for several weeks.

During the three successive treatments of $HT-Li_2CuO_2$ with the Br_2 solution, the XRD intensities due to this phase progressively decreased while a new set of peaks, whose angle positions match those expected for monoclinic $LiCuO_2$, increased in intensity (Figure 2b−d). After the third leaching step, only the $LiCuO_2$ peaks are spotted on the XRD pattern (Figure 2d), and both peaks intensities and cell parameters (a = 5.721(3) Å, b = 2.727(2) Å, c = 5.653(8) Å, β = 120.96(6)°) are in good agreement with previous works.[13] The concentration of the Br_2 solution and the leaching time are found to be critical parameters for the successful preparation of $LiCuO_2$ phase since too long a reaction time and/or too concentrated a Br_2 solution resulted in the formation of $LiCuO_2$ along with large amounts of CuO and Li_2CuO_2 impurities. By merging analytical data (Li/Cu ratio and mean Cu o.s.) for different $LiCuO_2$ batches, the overall compositions of our leached samples are found to be close to $Li_{0.95}CuO_{1.95}$. In the following, these samples will be denoted as $LiCuO_2$. Generally, excessive leaching results in the formation of CuO and thus in lower Li/Cu and O/Cu

(19) Morcrette, M.; Leriche, J-B.;Patoux, S.; Wurm, C.; Masquelier, C. *Electrochem. Solid-State Lett.* **2003**, *6* (5), A80−A84.
(20) Brunauer, S.; Emmett, P. H.; Teller, E. *J. Am. Chem. Soc.* **1938**, *60*, 309.
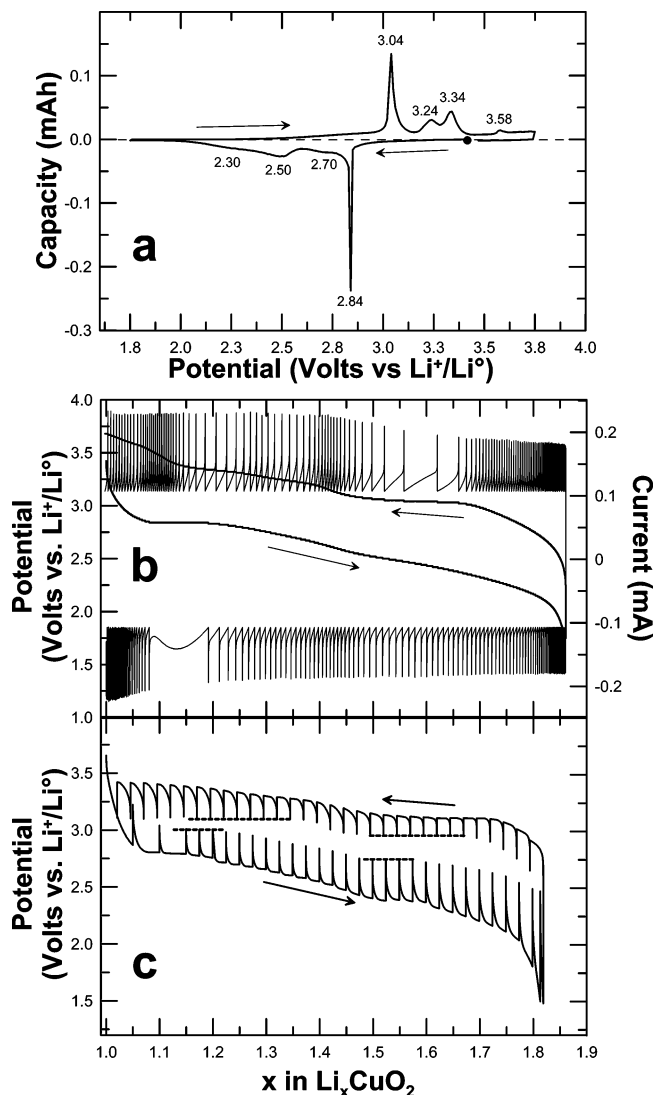
Figure 7. LiCuO₂/Li cell: (a) incremental dx/dV capacity obtained by integration of the chronoamperometric titration curve, (b) current and voltage evolutions as a function of the number of exchanged electrons, in a PITT mode (voltage step: 10 mV, equivalent limit current: 1 Li/20h), (c) voltage−composition curves in GITT mode (1Li/10h, 20 °C). The OCV (open circuit voltages) at quasi-equilibrium were recorded when the time evolution of the voltage was lower than 3 mV/h. Horizontal dashed lines indicate the constant OCV ranges.

ratios. Finally, nitrogen isotherm (77 K) adsorption data revealed a significant increase in the powder specific surface area during the leaching, namely, from less than 1 m²/g (Li₂CuO₂) to 6 m²/g (LiCuO₂). This was confirmed by SEM observations showing large, dense, and smooth Li₂CuO₂ particles of 2−20 μm in length (Figure 3a), while leached LiCuO₂ samples exhibit strongly exfoliated particles (Figure 3b). For instance, such exfoliation can account for the strong preferential orientation that we deduced from the Rietveld analysis of our XRD patterns. Also, assuming this high anisotropic texture is mirrored at a smaller intimate scale, it could also explain the important broadening of most of the XRD peaks (i.e., small crystallographic coherent domains) for LiCuO₂. Global EDS analysis confirms the absence of elemental impurity, such as Br, within the threshold determination of our apparatus (about 1 at. %, for elements with Z > 11).

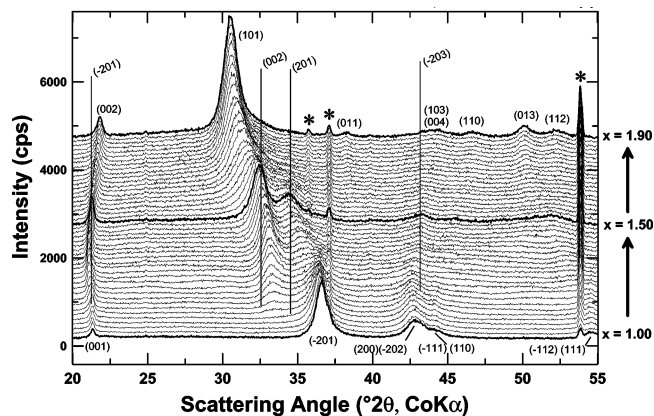Contrary to Li₂CuO₂, we observed a fast progressive decomposition for LiCuO₂ when exposed to air at ambient

Figure 8. In situ X-ray diffraction patterns collected on a LiCuO₂/Li cell discharged at a C/20 rate. Vertical bars and related italic indexation indicate the peak positions for the Li₁.₅CuO₂ phase. Asterisks indicate the peaks due to cell parts (Be). Bottom and top indexations are for LiCuO₂ and Li₂CuO₂, respectively. Each scan corresponds to an increment of 0.02 Li per formula unit.

Figure 9. In situ X-ray diffraction patterns collected during the charge (C/20) of a LiCuO₂/Li cell previously discharged up to x = 2 in Li$_x$CuO₂. Vertical bars and italic indexation indicate the peak positions for the Li₁.₅CuO₂ phase. Asterisks indicate peaks due to cell parts (Be). Bottom and top indexations are for Li₂CuO₂ and LiCuO₂, respectively. Each scan corresponds to an increment of 0.02 Li per formula unit.
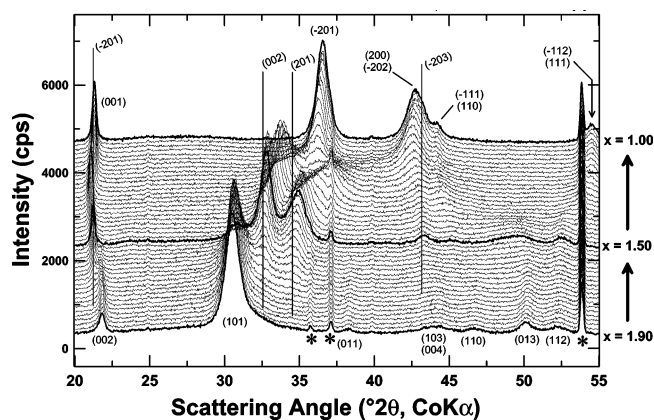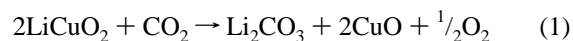
temperature (Figure 4). Freshly prepared LiCuO₂ (Figure 4a) decomposes into a mixture of CuO and Li₂CO₃ (Figure 4b) after several days of air exposure; Li₂CO₃ most likely originates from the reaction of lithia (Li₂O) with atmospheric moisture and carbon dioxide. Thus, the overall reaction of decomposition can be written as follows:

$$2LiCuO_2 + CO_2 \rightarrow Li_2CO_3 + 2CuO + {}^1\!/_2O_2 \qquad (1)$$

The same material being found to be very stable when stored in an argon atmosphere (Figure 4c), electrochemical measurements in an inert atmosphere can be performed without any risk of decomposition.

The thermal instability of both LiCuO₂ and Li₂CuO₂ under open air was also checked by high-temperature X-ray diffraction (HT-XRD) whose results are shown in Figures 5 and 6, respectively. Above 150 °C, LiCuO₂ starts to irreversibly transform into a mixture of Li₂CO₃ and CuO, similarly to what one observed upon exposure to air (Figure 5). At 250 °C, the decomposition reaction is completed and only thermally induced shifts of some reflections can be noted above this temperature. HT-Li₂CuO₂ was also found to be unstable upon air heating (Figure 6). Reflections due
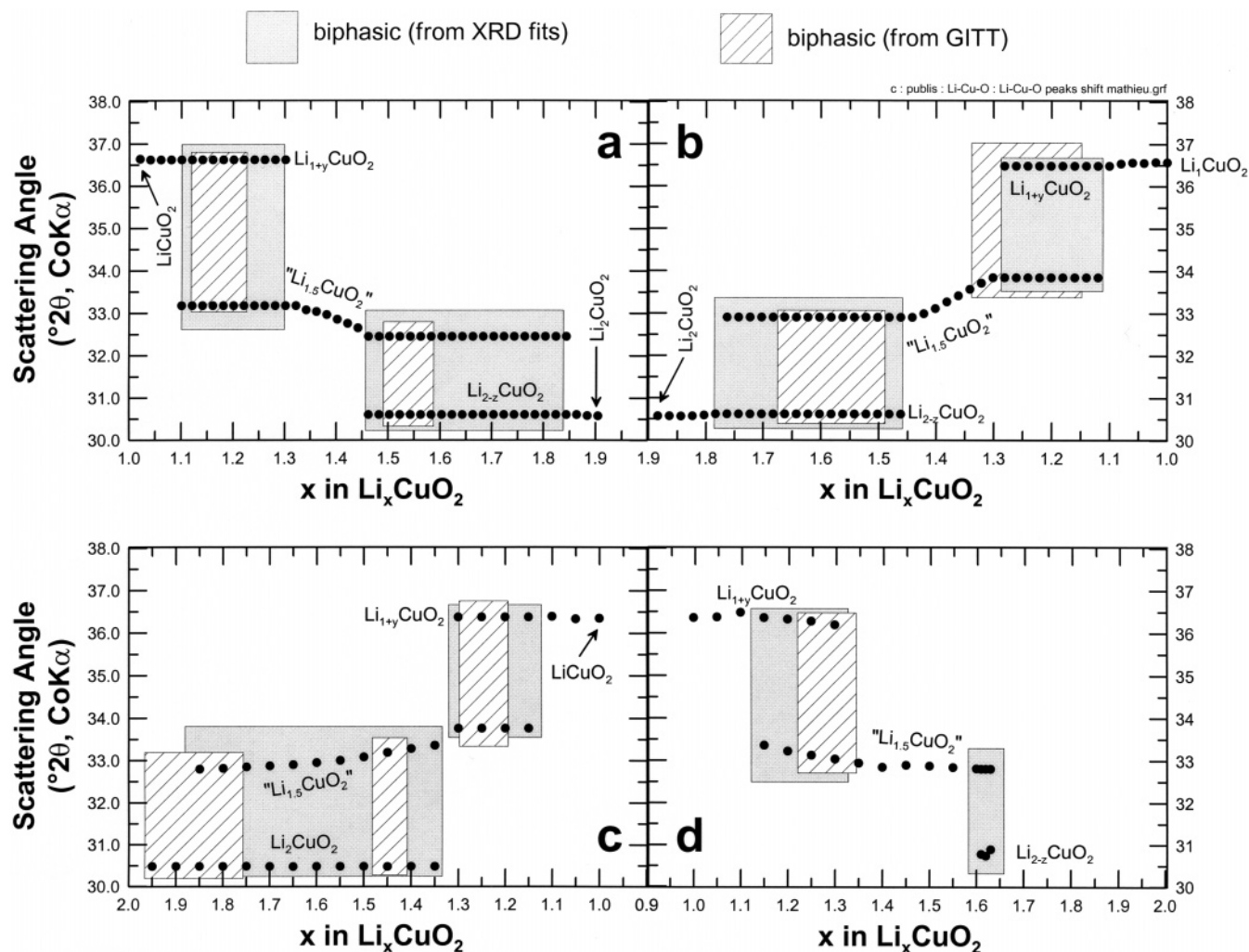
Figure 10. Evolution in the peak positions for each main reflection of each of the three type phases involved in the discharge (a) and charge (b) of the in situ LiCuO₂/ Li cell and during the charge (c) and discharge (d) of a Li₂CuO₂/Li in situ cell. In the computed range (30−37° 2θ, Co Kα), the selected reflections are (−201), (002), and (101) for LiCuO₂, Li₁.₅CuO₂, and Li₂CuO₂, respectively.

to CuO start appearing at 100 °C, with a continuous growth up to 325 °C together with increasing amounts of LiOH and Li₂CO₃. This decomposition therefore proceeds differently from that of LiCuO₂. First, the formation of LiOH + Li₂CO₃ instead of Li₂CO₃ only likely originates from the complex kinetically controlled reaction regarding the formation of lithium carbonate from LiOH/Li₂O. That formation is mainly altered by the surface area of contact and also implies the drastic role of the amount and rate of hydration of the sample.[21] Second, this decomposition is partial and even reversible, Li₂CuO₂ being indeed formed back at higher temperatures (>700 °C) without any trace of either CuO or Li salts, the only difference with the initial quenched sample (35 °C) being a global peak shift due to thermal expansion. When slowly cooled back to ambient temperature, Li₂CuO₂ partially decomposes into CuO + Li₂CO₃, demonstrating the metastability of the Cu ternary phase and thus the positive stabilization effect of the presently applied quenching from 500 °C during the synthesis. These results are far from being totally interpreted but nevertheless allow us to understand the presence of residual CuO in slowly cooled samples while we never observed such impurity in quenched ones. Since

(21) Wang, T. C.; Bricker, J. L. *Environ. Int.* **1980**, *2* (4−6), 425−430.

no lithium carbonate was found in quenched samples, we believe the formation of amorphous Cu−O side phase is unlikely.

Electrochemical Characterization: LiCuO₂. Incremental capacity data obtained by integration of the chronoamperometric titration curve for a LiCuO₂/Li cell (Figure 7a) reveals four steps for the first reduction (electrochemical insertion of Li⁺): a very sharp incremental peak at 2.84 V vs Li⁺/Li⁰, followed by three broad signals centered at about 2.7, 2.5, and 2.3 V vs Li⁺/Li⁰. The reoxidation step also consists of four signals, more distinct, and located at 3.04, 3.24, 3.34, and 3.58 V vs Li⁺/Li⁰. Biphasic processes being characterized by constant OCV (GITT) and by bell-shape/sigmoidal current evolution with time (PITT) while monophasic processes are clued by monotonic OCV evolution, a careful observation of Figures 7b and 7c can help in identifying the nature of these processes. Along the reduction, monophasic domains are spotted from x = 1.0 to x = 1.1 (x in Li_xCuO₂; no peak detected in Figure 7a), from x = 1.2 to x = 1.5 (broad signal centered at 2.70 V vs Li⁺/Li⁰) and from x = 1.6 down to the end of the discharge (broad signal centered at 2.30 V vs Li⁺/Li⁰). Thus, only two short biphasic domains at x = 1.1− 1.2 (2.84 V) and at x = 1.5−1.6 (2.50 V) seem to be crossed.
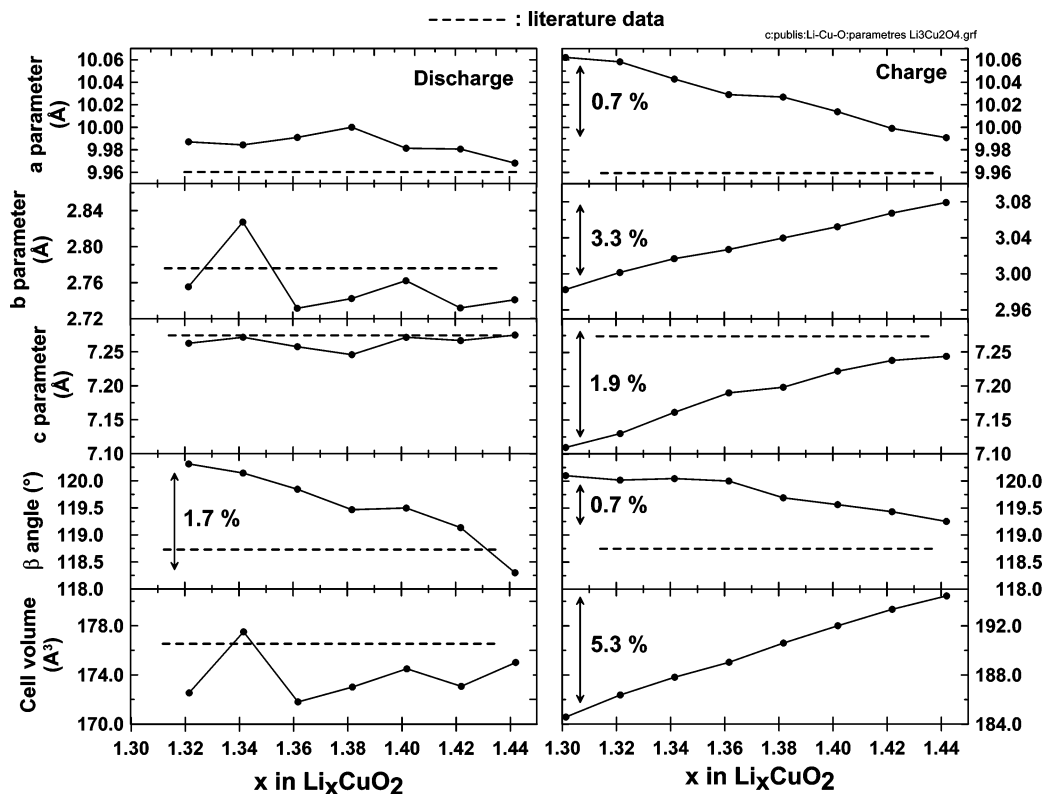
Figure 11. Evolution in cell parameters for the "Li$_{1.5}$CuO$_2$" phase within its monophasic domain of stability ($x = 1.3-1.45$) during charge and discharge of a LiCuO$_2$/Li in situ cell (C/20).
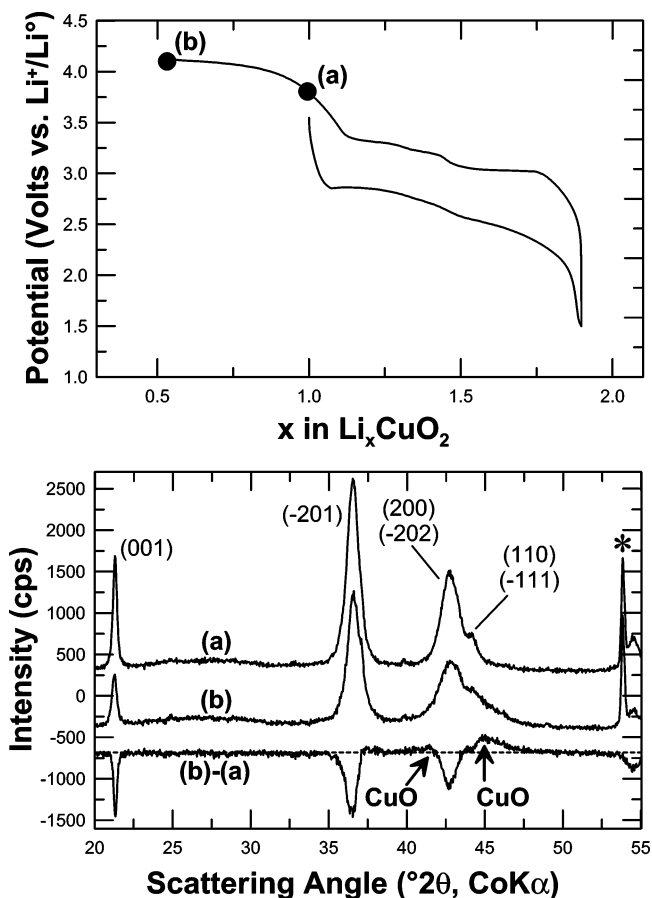

Figure 12. Complete galvanostatic voltage−composition curve for the in situ LiCuO$_2$/Li cell (top) and scan difference showing the growth of badly crystallized CuO during high-voltage charge (bottom). Asterisk indicates a peak due to the beryllium window.

Upon charge, the system does not behave in a strictly reversible manner since it presents extended biphasic domains ($x = 1.7-1.5$ at 3.04 V, $x = 1.35-1.15$ at 3.34 V) linked by limited monophasic domains ($x = 1.5-1.35$ and a broad signal centered at 3.24 V, and $x = 1.8-1.7$ with no peak in Figure 7a). Because of a very different voltage evolution in GITT and PITT modes at the very end of the charge, we found it difficult to assign the related capacity to any mechanistic process and to attribute the small incremental peak at 3.58 V. At first sight, such high voltage would let us suggest that it corresponds to the side formation of CuO, as previously discussed in the synthesis description.

To better understand the overall reaction and intermediate phase identification, in situ XRD experiments were undertaken. The collected patterns are displayed in Figure 8 (discharge) and Figure 9 (charge). Note that the constant peak position of the cell hardware (beryllium) rules out the eventuality of an artifact shift due to cell displacement during the experiment. Also worth pointing out is the very low relative peak intensity at low angle compared to the expected one and previous data (see Figure 2), which is due to the absorption of the Be window at grazing angles. First, after a very slight shift of the LiCuO$_2$ Bragg peaks at the very early stage of the reduction (e.g., formation of Li$_{1+y}$CuO$_2$ with $0 \leq y \leq 0.1$), this monophasic step is followed by the growth of a new set of peaks that can be related to a "Li$_{1.5}$CuO$_2$"-type phase. Then, from $x = 1.3$, these new reflections progressively shift toward the peak positions of stoichiometric Li$_{1.5}$CuO$_2$ to finally reach them at $x = 1.45$. Finally, upon further reaction with lithium, this phase appears to progressively transform into Li$_{2-z}$CuO$_2$ and then finally Li$_2$CuO$_2$. During the oxidation step, the same
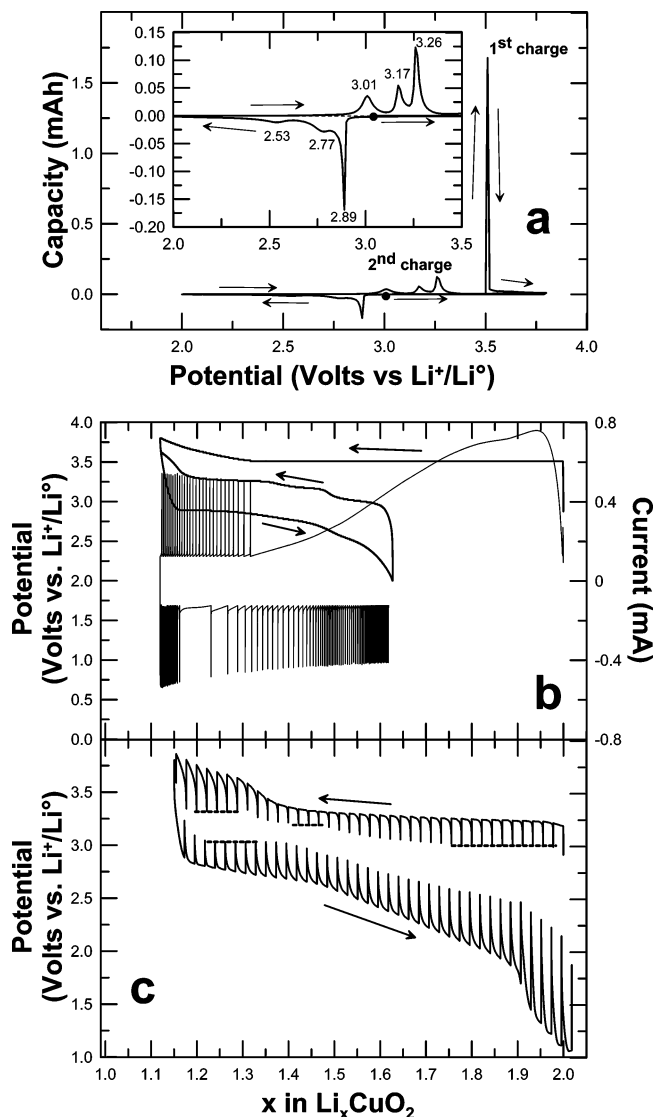
Figure 13. Li_2CuO_2/Li cell: (a) incremental dx/dV capacity obtained by integration of the chronoamperometric titration curve, (b) current and voltage evolutions as a function of the number of exchanged electrons, in PITT (potentiostatic intermittent titration technique) mode (voltage step: 10 mV, equivalent limit current: 1 Li/20h), and (c) voltage–composition curves in GITT mode (1Li/10h, 20 °C). The OCV (open circuit voltages) at quasi-equilibrium were recorded when the time evolution of the voltage was lower than 3 mV/h. Horizontal dashed lines indicate the constant OCV ranges.

sequence of type phases is observed whereas some differences can already be detected in peak positions for the "$Li_{1.5}CuO_2$" phase.

To grasp more details about these successive transformations, all the collected patterns were fitted, and a summary of the resulting data is presented in Figures 10a and 10b where the evolution in position for each main diffraction peak of the three structural types ((−201) for $Li_{1+y}CuO_2$, (002) for "$Li_{1.5}CuO_2$", and (101) for $Li_{2-z}CuO_2$) is plotted as a function of the number of reacted lithiums per copper. Aside from the confirmation of the sequence of monophasic–biphasic processes already proposed from electrochemical titrations, a comparison between Figure 7 and Figures 10a and 10b reveals an apparent mismatch with large discrepancies in the composition ranges for the stability of the different phases formed along the discharge and charge of the cell. For instance, the extent of the "$Li_{1.5}CuO_2$"–$Li_{2-z}CuO_2$ biphasic domain is evaluated to $\Delta x = 0.1$ and
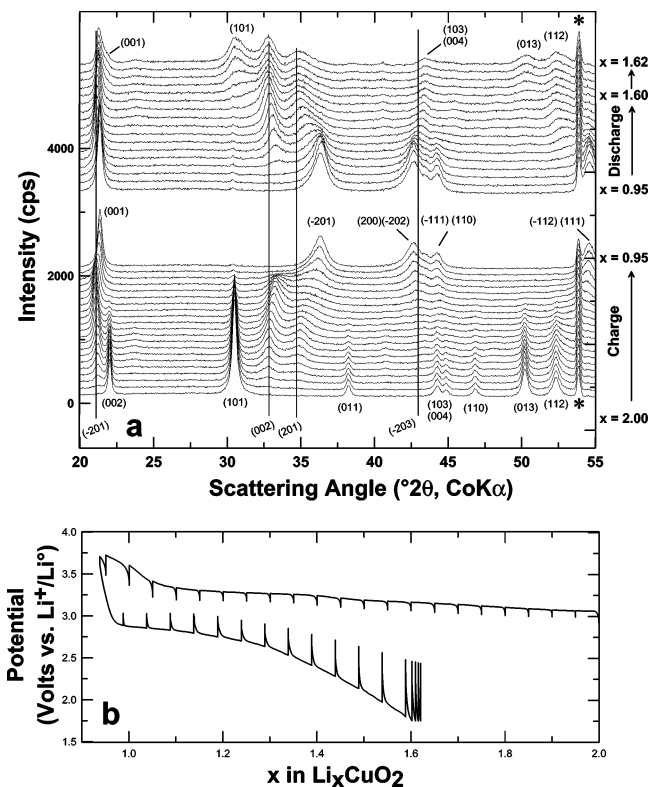

Figure 14. (a) In situ X-ray diffraction patterns collected during the charge and discharge of a Li_2CuO_2/Li cell (C/20, 20 °C). Vertical bars and italic indexation indicate the peak positions for $Li_{1.5}CuO_2$ phase. Asterisk indicates a peak due to cell parts (Be). Scans were collected during each relaxation step applied after capacity increment of 0.05 Li (1Li/20h) per formula unit. (b) Corresponding voltage–composition curve. Note the drastic increase in polarization during the last part of the reduction.

$\Delta x = 0.4$ from GITT and from in situ XRD analysis, respectively.

No noticeable difference can be spotted either for $Li_{1+y}CuO_2$ or for $Li_{2-z}CuO_2$ phases, based on their peak positions along charge and discharge sweeps. In contrast, the situation is totally different for "$Li_{1.5}CuO_2$" with a global shift of half a degree toward higher angles from the charge to the discharge sweep, for identical lithium contents (Figures 10a and 10b). This suggests some differences in the intimate reaction process for the formation of "$Li_{1.5}CuO_2$" from $Li_{2-z}CuO_2$ and from $Li_{1+y}CuO_2$. Far from being totally understood, this point can nevertheless be illustrated by the cell parameters evolution within the monophasic domain for "$Li_{1.5}CuO_2$" (i.e., $x = 1.3-1.45$). This is shown in Figure 11 which reveals, upon discharge, a monotonic change for the β angle only, while a, b, and c parameters are either quasiconstant or changing in a nonhomogeneous way. Upon charge, the "$Li_{1.5}CuO_2$" phase transforms through a monotonic evolution of the cell parameters (b and c decrease, a and β increase) with a resulting volume expansion of 5.3%. From these data, it is clear that the main difference between the "$Li_{1.5}CuO_2$" phase formed upon charge and discharge is nested in the value of the b parameter (2.98–3.08 Å on charge, 2.73–2.83 Å on discharge), which is also the one exhibiting the most important variations within the monophasic domain (3.3%). Therefore, combined value and evolution in this cell parameter drive the important differences observed in cell volume.
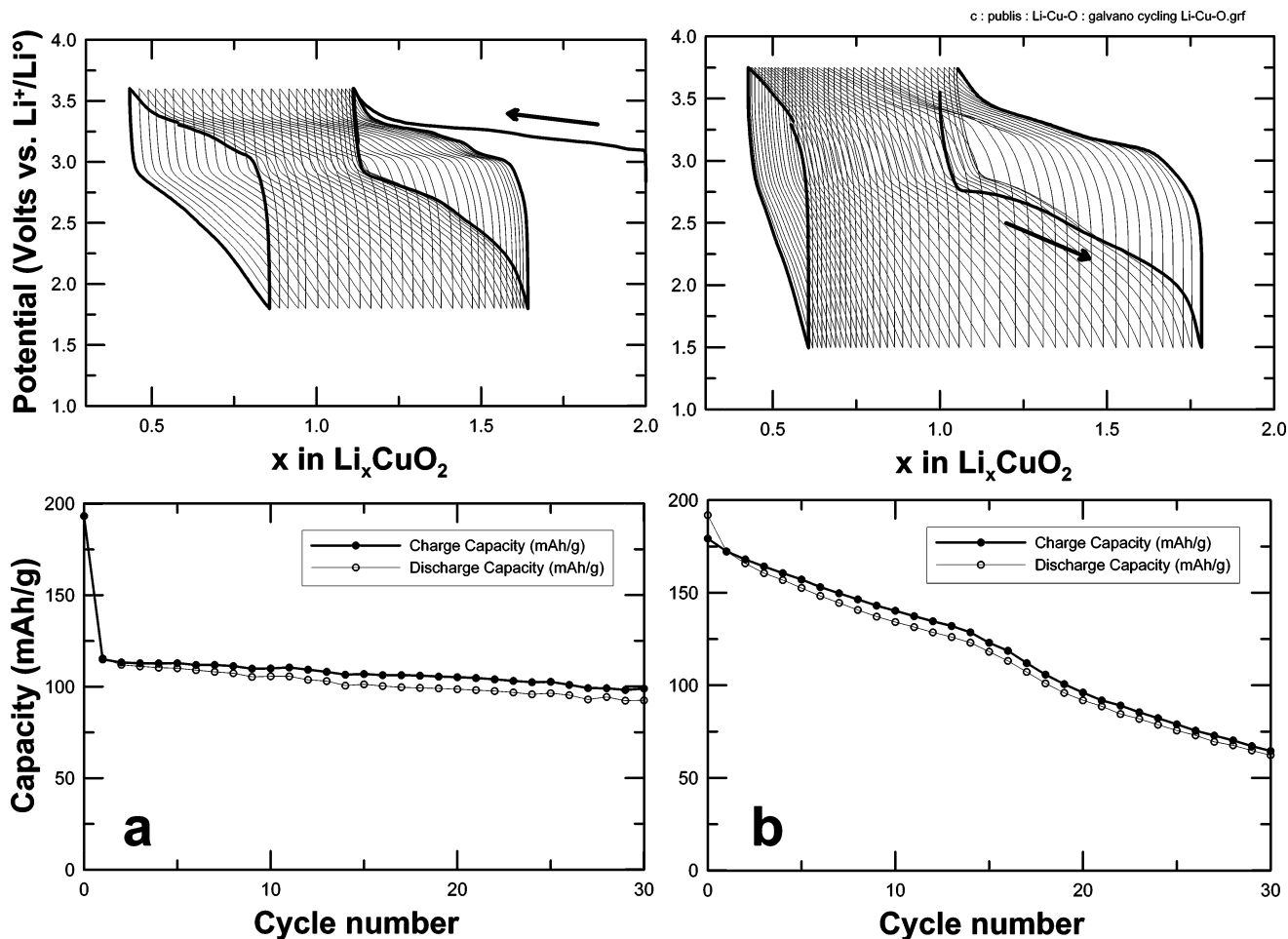
Figure 15. Cycling galvanostatic voltage−composition curves (1Li/5h, 20 °C) and evolution in charge and discharge capacities as a function of the cycle number for Li_2CuO_2/Li (a) and $LiCuO_2/Li$ (b) cells. Bold lines indicate first and last recorded cycles.

At about 3.8 V vs Li^+/Li^0, pure $LiCuO_2$ being totally recovered, the reaction is therefore found to be globally reversible. Once $LiCuO_2$ is formed, the charge can be pushed up to higher voltages, leading to the partial decomposition of $LiCuO_2$ into badly crystallized CuO, as evidenced by the scans difference presented in Figure 12. This confirms the results of over leaching/oxidation step during the synthesis, data presented in ref 5, and can also account for the unexplained features and discrepancies observed at the end of the charges (Figures 7 and 13).

Electrochemical Characterization: Li_2CuO_2. Keeping in mind the apparent one-step chemical oxidation (Figure 2) vs the multistep electrochemical oxidation of Li_2CuO_2, and based on the phases sequence during the reduction/oxidation of $LiCuO_2$, we tested the electrochemical reactivity of Li_2CuO_2 itself. A typical PITT signature of a Li_2CuO_2/Li cell (Figures 13a and 13b) mainly shows a very long biphasic process at 3.5 V vs Li^+/Li^0 from $x = 2.0$ to $x = 1.3$ followed by a sloppy voltage evolution up to $x = 1.1$. The discharge curve has a more complex shape entailing a sequence of three distinct phenomena (inset Figure 13a) very similar to the first discharge of a $LiCuO_2/Li$ cell (Figure 7a). Due to a drastic voltage drop at $x = 1.6$ for a 2.0 V cutoff voltage, the last "$Li_{1.5}CuO_2$" → $Li_{2-z}CuO_2$ transformation was very limited, hence the non-noticeable 2.30 V signal. Instead of a long voltage plateau, the second charge also shows a sequence of three phenomena in the 3.0−3.5 V range, the

voltage positions of which perfectly match those of the charge for a pre-discharged $LiCuO_2/Li$ cell. However, compared to the other two signals, the relative intensity of the charge signal at 3.01 V for a Li_2CuO_2/Li cell (Figure 13a) is much smaller than that of the 3.04 V for a $LiCuO_2/Li$ cell (Figure 7a). This can be explained by a very limited amount of $Li_{2-z}CuO_2$ formed at the end of the drop discharge, hence the limited extent of the $Li_{2-z}CuO_2$ → "$Li_{1.5}CuO_2$" back reaction. Assuming that the large differences between the first charges curves for $LiCuO_2/Li$ and Li_2CuO_2/Li cells as well as the shortened discharge sweep originate from kinetic limitations due to larger particle/crystallite size for Li_2CuO_2 than for $LiCuO_2$, one would expect a more distinct signature from galvanostatic titration and OCV values. This is indeed what is observed in Figure 13c with a succession of biphasic/monophasic domains on charge, a high-voltage feature likely linked to the onset of decomposition into CuO, and a much longer discharge reaching $x = 1.8$ at 2.0 V vs Li^+/Li^0.

The corresponding phase evolution followed by in situ XRD (Figure 14) revealed the participation of the same three type phases as detected in the case of $LiCuO_2$ with an evolution in positions for the main respective reflections (Figure 10c and d). From these data, it is clear that the Li_2-CuO_2 → $LiCuO_2$ transformation implies extended biphasic domains interconnected by very short solid solutions. The shift of the "$Li_{1.5}CuO_2$" Bragg peaks concomitant with the

vanishing of those of Li$_2$CuO$_2$ can also be understood by kinetics limitation and nonequilibrium states. Finally, well-crystallized LiCuO$_2$ is formed at the end of the charge at 3.8 V vs Li$^+$/ Li^0. During the subsequent discharge, "Li$_{1.5}$-CuO$_2$" is again found as an intermediate, but Li$_{2-z}$CuO$_2$ is barely detected at 2.0 V whereas for LiCuO$_2$, the transformation is completed at this voltage. Another proof of kinetic limitations in this system is provided by the large and progressive increase in polarization during the discharge (Figure 14b), together with the growth of Li$_{2-z}$CuO$_2$ from "Li$_{1.5}$CuO$_2$" promoted by applying repeated discharge steps stopping at 1.75 V without any significant further Li uptake. Under galvanostatic mode, it is necessary to push the reduction down to 1.3 V vs Li$^+$/Li^0 to recover pure divalent oxide.

Overall Reversibility: Li$_2$CuO$_2$ vs LiCuO$_2$. The cycling of both LiCuO$_2$ and Li$_2$CuO$_2$ was tested in galvanostatic mode (Figure 15) with cutoff voltages of 3.8 V and 1.5–1.75 V vs Li$^+$/Li^0. From these results, it is obvious that the capacity retention is much better for Li$_2$CuO$_2$ than for LiCuO$_2$, although the overall maintained capacity is much lower (100 mAh/g) than the initial charge length (190 mAh/g). Since the major difference between these two experiments resides in the limitation of the "Li$_{1.5}$CuO$_2$" ⇆ Li$_{2-z}$CuO$_2$ transition, it suggests that this step is highly detrimental to the electrochemical reversibility in this system.

Conclusions

In contrast to the direct Li$_2$CuO$_2$ → LiCuO$_2$ transformation observed by optimized chemical oxidation, a series of biphasic and monophasic transformations were found to take place along the electrochemical charge/discharge steps for Li$_2$CuO$_2$/Li and LiCuO$_2$/Li cells. These transformations systematically involve three type phases: Li$_{1+y}$CuO$_2$, "Li$_{1.5}$-CuO$_2$", and Li$_{2-z}$CuO$_2$. The long-term reversibility of these reactions was found to be highly dependent on the selected transitions, a much better capacity retention (100mAh/g, 30 cycles) being reached when one constrains the cycling on the LiCuO$_2$ ⇆ Li$_{1.5}$CuO$_2$ transition. Although some aspects of these reactions are not yet fully understood, it demonstrated that electrochemically Li-driven reactions can be a very convenient way to pave the way for mixed-copper valence phases with various compositions and structures. This is of special interest in view of magnetism and conductivity investigations. Finally, this study confirmed the intrinsic irreversible thermal and air instabilities for LiCuO$_2$, and also enlightened the metastable character of Li$_2$CuO$_2$ with very low onset temperature of about 150 °C.